Applied Catalysis B: Environmental 234 (2018) 223–233

Contents lists available at ScienceDirect

Applied Catalysis B: Environmental

journal homepage: www.elsevier.com/locate/apcatb

Cu-Al_2O_3-g-C_3N_4 and Cu-Al_2O_3-C-dots with dual-reaction centres for simultaneous enhancement of Fenton-like catalytic activity and selective H_2O_2 conversion to hydroxyl radicals

Suqian Xu[a], Hanxu Zhu[a], Wenrui Cao[b], Zhibin Wen[a], Jinnan Wang[a,*], Corvini Philippe François-Xavier[c], Thomas Wintgens[c]

[a] State Key Laboratory of Pollution Control and Resource Reuse & School of the Environment Nanjing University, Nanjing 210023, China
[b] Key Laboratory for Water Quality and Conservation of the Pearl River Delta, Ministry of Education, Institute of Environmental Research at Greater Bay, Guangzhou University, Guangzhou 510006, China
[c] School of Life Sciences, University of Applied Sciences and Arts Northwestern Switzerland, Basel 4132, Switzerland

ARTICLE INFO

Keywords:
Cu-Al_2O_3-g-C_3N_4
Cu-Al_2O_3-C-dots
Dual-reaction centres
Catalytic activity
H_2O_2 utilization

ABSTRACT

Cu-Al_2O_3-g-C_3N_4 and Cu-Al_2O_3-C-dots were synthesized for the first time to enhance the catalytic activity and utilization of H_2O_2. SEM, TEM, XPS, FT-IR, XRD, TPR and solid-state EPR were used to characterize the catalysts. In the Cu-Al_2O_3-g-C_3N_4 system, the electron-rich centre of Cu and electron-deficient site of Al were formed due to the higher electronegativity of Cu. Moreover, Cu ions could coordinate with the hydroxyl on the tri-s-triazine ring of g-C_3N_4 or the graphene conjugated π-domains of C-dots via the Cu−O−C linkage so that the orbital interactions involving electron transport from π → Cu also induced the formation of an electron-rich Cu centre and an electron-deficient π-electron conjugated system, resulting in the strengthening of the dual-reaction centres. This mechanism was validated by Roman, EPR and XPS spectra. In addition, EPR experiments demonstrated that two electron-transfer processes formed ·OH in the presence of H_2O_2. The first electron transfer was from the electron-rich Cu centres to H_2O_2, and the other was from H_2O to the electron-deficient site. Thus, more ·OH were generated and high H_2O_2 utilization was achieved in the Cu-Al_2O_3-g-C_3N_4 and Cu-Al_2O_3-C-dots suspension. Furthermore, the turnover frequency (TOF) for the Cu-Al_2O_3-C-dots and Cu-Al_2O_3-g-C_3N_4 dispersions were determined and were found to be much higher than those of the classic homogeneous Fenton reaction. Thus, Cu-Al_2O_3-g-C_3N_4 and Cu-Al_2O_3-C-dots showed high activity and stability for the catalytic degradation of organic pollutants under mild conditions.

1. Introduction

Although the classical homogeneous Fenton reaction has been widely used for the degradation of organic pollutants [1], problems such as narrow pH range (2–3), loss of the catalyst and the accumulation of iron precipitates still remain to be resolved [2]. To overcome these disadvantages, many researchers have investigated the preparation of efficient heterogeneous Fenton-like catalysts, which could be applied in a relatively wide pH range to replace the homogeneous Fenton process [3–5]. During the Fenton reaction, H_2O_2 can not only react with the reduced metal (M^{n+}) as the electron acceptor but also reacts with the oxidized metal [$M^{(n+m)+}$] as the electron donor, accompanied by the circulation of $M^{n+}/M^{(n+m)+}$ and the generation of ·OH or HO_2· [6]. However, for the most widely used Fenton system (H_2O_2 and Fe^{2+}), the rate constants (0.001–0.02 $M^{-1}s^{-1}$) of H_2O_2 reduction of Fe^{3+} to Fe^{2+} are relatively low, significantly restricting the Fe^{3+}/Fe^{2+} circulation [7]. Thus, various methods including isomorphic doping of transition metals and use of UV/vis light irradiation have been investigated to improve the valence state cycles [8,9], in spite of the inevitable increases in the cost and energy consumption during the water/wastewater treatment process incurred by these additional enhancement methods [10,11]. In an alternative approach, copper, which has similar redox properties to iron and which in its Cu (II) from can be more easily reduced by H_2O_2 with a high kinetic constant (Eqs. (1) and (2)), can be used in a Fenton-like system [12,13]. Notably, compared to Fe^{3+}, Cu^{2+} complexed with organic degradation intermediates (organic acids) was more easily decomposed by HO· [14,15], which was beneficial to the Cu^{2+}/Cu^{+} circulation. In addition, the copper complex $[Cu(H_2O)_6]^{2+}$ was soluble at neutral pH conditions, enabling the use of the Cu^{2+}/H_2O_2 Fenton-like system in a broad

* Corresponding author.
E-mail address: wjnnju@163.com (J. Wang).

https://doi.org/10.1016/j.apcatb.2018.04.029
Received 18 January 2018; Received in revised form 3 April 2018; Accepted 16 April 2018
Available online 17 April 2018

pH range. Thus, the Cu^{2+}/H_2O_2 Fenton-like system has attracted much research interest.

$$Cu^{2+} + H_2O_2 \rightarrow Cu^{+} + HO_2\cdot + OH^{-} \quad (k = 4.6 \times 10^2\ M^{-1}\,s^{-1}) \qquad (1)$$

$$Cu^{+} + H_2O_2 \rightarrow Cu^{2+} + HO\cdot + HO^{-} \quad (k = 1.0 \times 10^4\ M^{-1}\,s^{-1}) \qquad (2)$$

However, in the classic Fenton system mentioned above (oxidation of hydrogen peroxide), a fraction of H_2O_2 could act as an electron donor and finally decomposed with the formation of O_2 and the superoxide radical ($O_2\cdot^{-}$). Since O_2 cannot directly degrade the organic pollutant, the utilization efficiency of H_2O_2 was relatively low. To enhance the selective H_2O_2 conversion to hydroxyl radicals, galvanic-like cells effects were used to facilitate the reduction of H_2O_2 to ·OH. Previous studies have demonstrated that the non-uniformity of the negative charge of the lattice oxygen could form galvanic-like cells in a lattice-doped silica nano-sphere composite due to the different electro-negativities of the doped metals (Ti, Cu, Al); therefore, almost the entire energy of H_2O_2 was used to degrade the organic pollutants, resulting in the high utilization of H_2O_2 [16]. Furthermore, a surface complex of Cu with hydroxyl on the aromatic ring of the carbon-doped g-C_3N_4 (OH-CCN/CuCo-Al_2O_3) was also applied to induce the formation of electron-rich Cu centre, in which two electron transfer routes were present upon addition of H_2O_2, with the transfer from electron-rich Cu centres to H_2O_2 to generate ·OH as the first route and the transfer from H_2O to the N atom of OH-CCN to produce ·OH as the second route [17]. Since cation-π interactions are considered to be important for intermolecular binding forces in the cation and aromatic systems [18], the charge transfer of transition-metal ions may be obviously influenced by the cation-π interactions.

On the other hand, owing to its tuneable electronic properties and excellent chemical stability, carbon nitride (g-C_3N_4) has been considered to be an important material for photocatalysis. Generally, g-C_3N_4 consists of 2D sheets of tri-s-triazine connected by tertiary amines in which the typical π-conjugated graphitic planes were formed via the sp^2 hybridization of carbon (C) and nitrogen (N) atoms [17]. Thus, incorporation of metallic elements into the g-C_3N_4 matrix could induce the production of delocalized electrons, promoting the catalytic reactions [19]. In addition, analogous to g-C_3N_4, owing to sp^2 and sp^3 hybridized carbons including hydroxyl, peripheral carboxylic and carbonyl moieties, carbon quantum dots (C-dots) have also been considered as a potential carbon-based material for use in photocatalysis [20,21]. The formation of an activated transition complex [CH_2O_2] during the H_2O_2 decomposition process, which can transfer electron density from the π-system of the C-dots to the peroxide molecule during the decomposition process of H_2O_2 [22].

Building on the research studies mentioned above, we synthesized two novel flower-like spherical catalysts (Cu-Al_2O_3-g-C_3N_4 and Cu-Al_2O_3-C-dots) with double catalytic active centres by hydrothermal reactions. In these catalysts, Cu was incorporated in the Al_2O_3 lattice and substitutes for Al, giving rise to the non-uniform electron density distribution of the lattice O^{2-} owing to the differences between the electro negativities of the metals. Owing to the bonding between the lattice O^{2-} with these metal atoms, a higher electron density was formed around Cu, while a lower electron density appeared in the region near Al, resulting in the formation of the dual-reaction centres. More importantly, we provided two simple and efficient ways to synergistically strengthen the dual-reaction centres. In the first approach, we constructed the Cu-Al_2O_3-g-C_3N_4 system in which the organic ligand coordinates with the Cu ions to induce the formation of an electron-rich Cu centre and decrease the electron density of the π-electron conjugated system through cation-π interactions. In the second approach, we introduced C-dots into Cu-Al_2O_3 to construct the orbital interactions involving electron transfer of π → Cu (σ donation), which could also promote the catalytic efficiency. To achieve this goal, our study focused on the following three main objectives: (1) the preparation and characterization of the catalysts (Cu-Al_2O_3, Cu-Al_2O_3-g-C_3N_4 and Cu-Al_2O_3-C-dots), especially the characterization of the formation of the dual-reaction centres by the solid and liquid electro paramagnetic resonance (EPR) techniques, (2) the testing of the catalytic activities using degradation of Bisphenol A (BPA), 2,4-dichlorophenoxyaceticacid (2,4-D), phenytoin (PHT) and two dyes [methylene blue (MB) and Rhodamine B (Rh B)], as well as the evaluation of the improvement of the H_2O_2 utilization, and (3) suggestion of the possible catalytic mechanisms.

2. Experimental

2.1. Materials

Glucose ($C_6H_{12}O_6$), aluminium nitrate nonahydrate ($Al(NO_3)_3{\cdot}9H_2O$), copper nitrate trihydrate ($Cu(NO_3)_2{\cdot}3H_2O$), hydrogen peroxide (H_2O_2, 30%, w/w) and urea were purchased from the National Medicines Corporation Ltd. of China. Horseradish peroxidase (POD), Rhodamine B (Rh B), Bisphenol A (BPA), methylene blue (MB), phenytoin (PHT) methanol, *N*,*N*-diethyl-*p*-phenylenediaminesulfate (DPD), 2,4-dichlorophenoxyaceticacid (2,4-D), terephthalic acid (TPA), and 5,5-Dimethyl-1-pyrrolineN-oxide (DMPO) were supplied by Aladdin Industrial Corporation, China. Graphite rods (99.99%) were purchased from Alfa Aesar Co. Ltd. Deionized water was used throughout this study. All chemicals were A. R. grade (> 99%) and were used without further purification.

2.2. Preparation of catalysts

2.2.1. Synthesis of g-C_3N_4 and C-dots

g-C_3N_4 was prepared following the method reported in the previous studies [23]. Typically, urea was added to an alumina crucible with a cover and then heated to 550 °C with the heating rate of 5 °C per minute in a muffle furnace. After heating for 3 h, the sample was cooled down to room temperature, and the product (g-C_3N_4) was obtained.

C-dots were synthesized according to the method of the previous studies [24]. Two parallel graphite rods connected with direct current (DC) power (15–60 V) were inserted into ultrapure water and acted as the anode and cathode, respectively. After continuous stirring for 5 days in the reactor, the colour of the solution gradually changed from transparent to dark yellow owing to the corrosion of the anode graphite rod. To obtain the C-dots solution, the precipitated graphite oxide and graphite particles were removed from the dark yellow solution by centrifugation (8000 rpm).

2.2.2. Synthesis of Cu-Al_2O_3, Cu-Al_2O_3-g-C_3N_4 and Cu-Al_2O_3-C-dots

2.2.2.1. Spherical flower-like Cu-Al_2O_3. 7.5 g of ($Al(NO_3)_3{\cdot}9H_2O$, 5.0 g of $C_6H_{12}O_6$, 0.604 g $Cu(NO_3)_2{\cdot}3H_2O$ and 60 mL of deionized water were added to a 150 mL flask with stirring at 25 °C for 1 h. Then, the suspension liquid was transferred into a 150 mL Teflon-lined autoclave and kept in a high temperature oven at 180 °C for 20 h. The obtained product was washed several times with deionized water and then calcined in a muffle furnace at 550 °C for 4 h at the heating rate of 5 °C per minute. To optimize the copper content, Cu-Al_2O_3 samples with various copper contents (3, 5, 7.8, and 9.1 wt %) were prepared in the present work. Since the subsequent catalytic performance experiments (Section 3.2) indicated that (7.8 wt%) Cu-Al_2O_3 exhibited the highest catalytic activity (Fig. 6B), 7.8 wt% copper content was selected to prepare Cu-Al_2O_3-g-C_3N_4 and Cu-Al_2O_3-C-dots. Furthermore, as reference, Fe-Al_2O_3 samples with the addition of $Fe(NO_3)_3{\cdot}9H_2O$ and Al_2O_3 were prepared following the same method.

2.2.2.2. Cu-Al_2O_3-g-C_3N_4. 7.5 g of $Al(NO_3)_3{\cdot}9H_2O$, 5.0 g of $C_6H_{12}O_6$, 0.604 g $Cu(NO_3)_2{\cdot}3H_2O$ and a certain dose of g-C_3N_4 were dissolved in 60 mL deionized water, and the procedures used in the subsequent synthesis steps were the same as in the synthetic process for Cu-Al_2O_3 described above. Moreover, to determine the optimal content of g-C_3N_4, Cu-Al_2O_3-g-C_3N_4 with various contents of g-C_3N_4 (1.5, 3.0, 4.5, 6.0 and 9.0 wt%) were prepared.

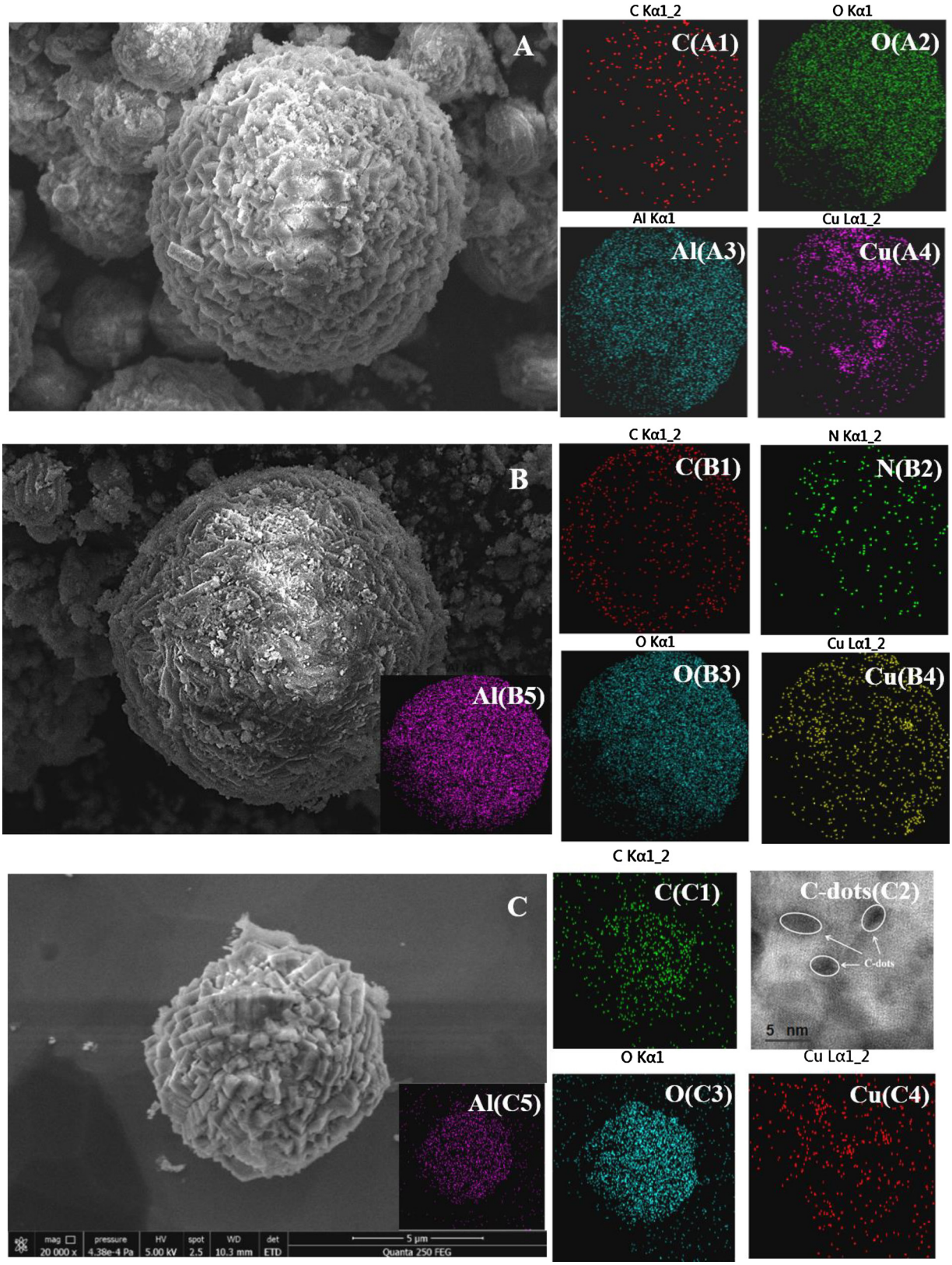

Fig. 1. Micrographs images of (A) Cu-Al_2O_3 and EDS element distribution of C, O, Al and Cu (B) Cu-Al_2O_3-g-C_3N_4 and EDS element distribution of C, N, O, Al and Cu (C) Cu-Al_2O_3-C-dots, EDS element distribution of C, O, Al and Cu, TEM image of C-dots in Cu-Al_2O_3-C-dots.

2.2.2.3. Cu-Al_2O_3-C-dots. 7.5 g of $(Al(NO_3)_3{\cdot}9H_2O$, 5.0 g of $C_6H_{12}O_6$, and 0.604 g $Cu(NO_3)_2{\cdot}3H_2O$ were dissolved in 18.3 mL of (0.1 g/L) C-dots stock solution, and a certain volume of deionized water was added in. The procedures for the subsequent synthesis steps were as same as in the synthetic process for Cu-Al_2O_3 mentioned above. Cu-Al_2O_3-C-dots with various contents of C-dots (0.05, 0.15, 0.2, 0.3, 0.4 and 0.5 wt%) were prepared to determine the optimal C-dots content.

2.3. Characterization methods

Surface morphology and distribution of the elements in the catalysts were characterized by transmission electron microscopy (TEM, JEM-200CX) and field emission scanning electron microscopy (FESEM, QUANTA FEG 250), respectively. To observe the crystal structure of the catalysts, X-ray diffraction (XRD) spectra were collected using a XRD-6000 X-ray diffractometer (Shimadzu, Japan) with a Cu K radiation (=1.5406 Å) over the 2θ range of 10–60°. The Brunner–Emmet–Teller (BET) specific surface area, pore diameter and pore volume of the catalysts were measured using a gas sorption analyser (NOVA2000e) at the liquid nitrogen temperature. In addition, the Fourier transform infrared spectra (FT-IR) of the KBr pelleted samples were recorded using a NEXUS870 FT-IR spectrometer, which could provide some useful information on the functional groups of the catalyst. To analyse the chemical state of the catalysts' surfaces, X-ray photoelectron spectroscopy (XPS) data were obtained with a PHI 5000 VersaProbe instrument using monochromatic Al Kα radiation (225 W, 15 mA, 15 kV). All binding energies were referenced to the C 1s peak at 284.2 eV. EPR spectra of the solid samples were obtained using the EMX-10/12 electron paramagnetic resonance spectrometer.

Furthermore, to characterize the redox properties of active materials (Cu) in catalyst composites, temperature-programmed reduction experiments were carried out with H_2 (TPR-H_2) using a Micromeritics Auto Chem II 2920 instrument with 0.1 mg of the catalyst heated at the rate of 10 °C/min from 40 °C to 700 °C under 5% H_2/Ar flow.

DMPO-trapped EPR signals were detected in different air saturated methanol/aqueous dispersions of the corresponding samples with and without the addition of H_2O_2. The detailed information for the recorded EPR signals of ·OH and $O_2\cdot^-$ is provided in the ESI.

In addition, the terephthalic acid (TPA) probe method was used to directly measure the concentration of ·OH in the aqueous dispersion with H_2O_2. Accordingly, the turnover frequencies (TOF) of Cu-Al_2O_3-g-C_3N_4, Cu-Al_2O_3-C-dots and Cu-Al_2O_3 were obtained from the conversion number of H_2O_2 into ·OH per second on a single active site. Detailed descriptions of the measurement of ·OH concentration by the TPA probe method and of the TOF calculation are provided in the ESI.

2.4. Catalyst performance

Five aromatic pollutants (BPA, 2,4-D, MB, Rh B, and PHT) were selected to evaluate the catalytic activity of the catalysts. Preliminary experiments for BPA degradation indicated that the optimal doses of the catalyst and H_2O_2 were 0.5 g/L and 12.5 mM, respectively (Fig. S7). Thus, these two doses were used in all catalytic degradation experiments unless otherwise specified. Typically, 200 mL aqueous solutions with a certain pollutant and 0.1 g of the catalyst were placed in 250 mL beaker flasks. To ensure the adsorption-desorption equilibrium, the suspensions were magnetically stirred for 30 min before the catalytic reaction. Then, 12.5 mM H_2O_2 was added in the suspensions with magnetic stirring (120 rpm). At given time intervals, 2 mL aliquots were sampled and filtered through a Millipore filter (pore size 0.45 μm) prior to the analysis. In addition, to test the catalytic stability of Cu-Al_2O_3-g-C_3N_4 and Cu-Al_2O_3-C-dots, the catalyst was recovered by filtration, washed with deionized water, dried and reused in the following cycle.

The concentrations of BPA, 2,4-D and PHT were analysed using a 1200 series HPLC equipped with a UV detector. Rh B and MB concentrations in solutions were analysed by recording the variations at the wavelength of the maximum absorption using a UV-1800 UV–vis spectrometer (Shimadzu, Japan). The H_2O_2 concentration was determined according to the DPD method reported in previous work [25]. In addition, an ICE3500 atomic absorption spectrometer (Thermo Scientific M) was used to measure the leaching of metallic ions into the solution during the entire reaction process.

3. Results and discussion

3.1. Morphology and structure of catalysts

SEM images indicate that all four products are flower-like spherical structure, and their surfaces are composed of cross-linked sheets (Fig. 1). Previous studies have reported a similar surface morphology of Al_2O_3 synthesized by the hydrothermal reaction. The formation of the flower-like spherical structure could be explained as due to the reaction of glucose with hydrated multi-nuclear aluminium hydroxides followed by gradual formation of lamellar inorganic-organic hybrid structures. Furthermore, EDS images also showed that the Al, Cu, O and C elements were almost homogenously distributed on the catalysts' surfaces. Unlike Al_2O_3 and Cu-Al_2O_3, Cu-Al_2O_3-g-C_3N_4 exhibits a partially fluffy surface, and a new element 'N' appears in the EDS image (Fig. 1B), suggesting that the g-C_3N_4 is well-exposed on the catalyst surface as sheet materials aggregate by self-assembly to form the flower-like spherical structures [26]. Although the EDS image cannot directly confirm the existence of C-dots on Cu-Al_2O_3-C-dots, the TEM image clearly demonstrates that the C-dots are well-dispersed on the Cu-Al_2O_3-C-dots (inset of Fig. 1C). In addition, Cu-Al_2O_3-C-dots showed more obviously flower-like structure and a rough surface.

The N_2 adsorption/desorption isotherms of Al_2O_3, Cu-Al_2O_3, Cu-Al_2O_3-g-C_3N_4 and Cu-Al_2O_3-C-dots are typical IV isotherms with the H3 hysteresis loop (Fig. S4A), indicating that the aggregation of the plate-like particles gives rise to slit-shaped pores [27]. The appearance of the hysteresis loop at p/p_0 = 0.5–0.9 and p/p_0 = 0.9–1.0, respectively, suggests the existences of meso-pores and macro-pores in the catalysts, which is also confirmed by the pore distribution (Fig. S4B). On the one hand, flower-like Al_2O_3 spheres were assembled by large amounts of disordered sheets composed of cyclic surfaces with many disordered pores and resulting in a high BET surface area and a porous structure. On the other hand, meso-pores also originated from the removal of uniform carbonized glucose materials in the inorganic–organic hybrid sheets and the stacking of the basic spherical units comprising the flower-like samples. Such meso-pore structure and high BET surface area were beneficial for the assembly of the pollutants on the catalyst surface, which could enhance the kinetics of the catalytic degradation process. In addition, C-dots and g-C_3N_4 doped in Cu-Al_2O_3 obviously increased the surface area while slightly decreasing the pore volume of the catalysts, which indicated that C-dots and g-C_3N_4 were not only exposed on catalysts surface but were also distributed inside the catalysts.

The XRD spectra indicate that the alumina substrate is found in an amorphous structure. After doping with Cu, new peaks at 32.5°, 38.7°, 35.4°, 48.8°, 53.4°, 58.5°, 62.3°, 65.8° and 68.1° appear (Fig. 2A–c), corresponding to the (110), (111), (002), (202), (020), (202), (-113), (002) and (220) planes of the CuO phase (JCPDs 65-2309), respectively. Although the characteristic peak of the C-dots at 24° is too weak to be observed owing to their low content (0.4%) (Fig. 2A–d), the TEM image still demonstrates the existence of C-dots of the Cu-Al_2O_3-C-dots (Fig. 1C2). Previous studies have also reported that a low content of C-dots could not be observed in the XRD spectra, owing to the relatively low diffraction intensity in the hybrid materials, and that TEM could be used to confirm the presence of C-dots [28]. The diffraction peak at 27.6° appeared in the Cu-Al_2O_3-g-C_3N_4 assigned to the characteristic (002) planes of graphitic carbon nitride.

FT-IR spectra (Fig. 2B) can provide more information regarding the catalysts functional groups. The peaks near 3458 cm^{-1} are ascribed to the stretching vibrations of OH [ν(OH)] in the water molecules adsorbed on the sample surface. Notably, compared to Cu-Al_2O_3 (3460 cm^{-1}), the ν(OH) shifted to a lower frequency (3455 cm^{-1} and 3457 cm^{-1}) in Cu-Al_2O_3-g-C_3N_4 and in Cu-Al_2O_3-C-dots, respectively. Based on previous reports, we could infer that the surface Cu was complexed by σ bonding to the oxygen atom of the hydroxyl group connected to the C of the aromatic ring in g-C_3N_4/C-dots [29], resulting

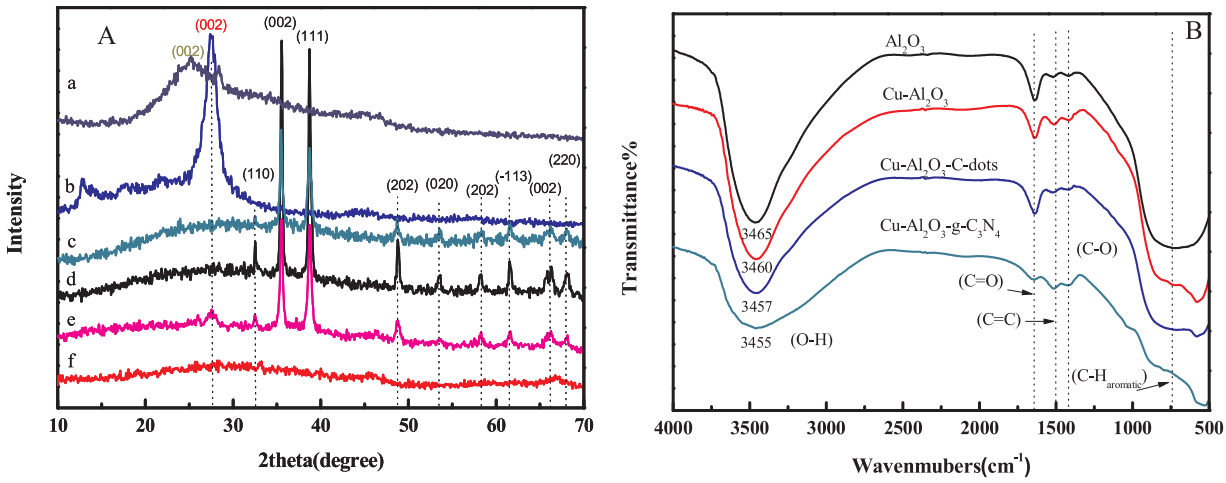

Fig. 2. (A) XRD patterns of the synthesized samples. (a) C-dots (b) g-C_3N_4 (c) Cu-Al_2O_3 (d) Cu-Al_2O_3-C-dots (e) Cu-Al_2O_3-g-C_3N_4 (f) Al_2O_3. (B) FTIR spectra of Al_2O_3, Cu-Al_2O_3, Cu-Al_2O_3-C-dots, Cu-Al_2O_3-g-C_3N_4.

in the formation of the C-O-Cu cross-linker from the combination of g-C_3N_4/C-dots and Cu–Al_2O_3. The peaks in the 1640–1650 cm^{-1} range were ascribed to C═O vibrations, whereas the bands in the 1515–1520 cm^{-1} range corresponded to C═C vibrations. In addition, the bands in the region of 1000–1450 cm^{-1} corresponded to C—O (hydroxyl, ester, or ether) [30]. Furthermore, the bands at 875–750 cm^{-1} were assigned to the out of plane bending vibrations of the aromatic C—H [31].

Generally, H_2-TPR is used to characterize the redox properties of catalysts. We observed two H_2 consumption peaks (at high temperature and low temperature) in the H_2-TPR of all samples, demonstrating the existence of copper ions with different redox behaviours (Fig. 3). The peaks of the four samples at 170–250 °C could be ascribed to the reduction of Cu(II)/Cu(I), which were well dispersed in catalysts and were easily reduced to Cu° ($Cu^{2+} + H_2 \rightarrow Cu + H_2O$ or $2Cu^{+} + H_2 \rightarrow 2Cu + H_2O$), while the peaks at 230–300 °C were assigned to the reduction of the larger size CuO particles, which were difficult to reduce. As the Cu content increased from 3 to 7.8 wt%, H_2 consumption peaks shifted towards lower reduction temperatures, together with a broader peak at low temperature. However, as Cu content increased from 7.8 to 9.0 wt%, H_2 consumption peaks shifted slightly to higher temperatures. This unusual phenomenon may be explained as follows: 1) since the sites of the Al_2O_3 framework limit the incorporation of copper, excess incorporation of copper led to more extra framework copper (larger CuO particles), which were more difficult to reduce, and 2) larger CuO particles may cover the copper atoms, which were dispersed in Al_2O_3 framework making their reduction more difficult. Thus, 7.8 wt% may be the optimal content of copper incorporation, which was also in accordance with the results of the degradation tests described in Section 3.2 (Fig. 6).

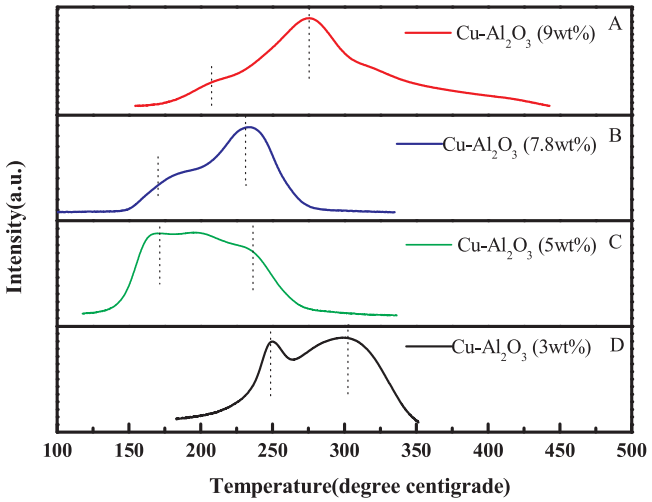

Fig. 3. TPR profile of different samples (A) Cu-Al_2O_3 (Cu: 9 wt%) (B) Cu-Al_2O_3 (Cu: 7.8 wt%) (C) Cu-Al_2O_3 (Cu: 5 wt%) and (D) Cu-Al_2O_3 (Cu: 3 wt%).

Furthermore, to explore the chemical state of the surface and the formation of chemical bonds in the composites, XPS spectra of the catalysts were analysed (Fig. 4). The two Al_2O_3 (Al 2p) peaks at 73.9 and 72.2 eV were assigned to Al—O—Al and Al/C of the flower-like Al_2O_3, respectively (Fig. S5A). After the incorporation of copper, three Al 2p peaks are observed (Cu-Al_2O_3, Cu-Al_2O_3-g-C_3N_4 and Cu-Al_2O_3-C-dots) (Fig. S5B–D). The peaks at 74.1–74.2 eV, 75.2–75.4 eV and 77.4–77.6 eV were ascribed to Al—O—Al, Al—O—Cu [32] and Cu $3p_{1/2}$, respectively. For the Cu 2p spectra (Cu-Al_2O_3, Cu-Al_2O_3-g-C_3N_4 and Cu-Al_2O_3-C-dots), the peaks at 932.1–932.3 eV, 934.1–934.9 eV and 941.2–941.4 eV correspond to the reduction state, oxidation state and fluctuation peaks of the copper species, respectively. Notably, Auger kinetic energy in the range of 570.2–573.7 eV further confirmed the existence of Cu^{+} rather than Cu° (Fig. 4E2 and F2).

For C 1s, the Al_2O_3 peaks at 284.6 eV and 288.1 eV may be ascribed to the carbon group (C—C) and carbonyl groups/quinone groups (> C═O), respectively (Fig. 4D). The peaks at 285.6–285.7 eV of Cu-Al_2O_3 and Cu-Al_2O_3-C-dots correspond to C—O (Fig. 4B and C). Notably, the peaks at 286.1 eV of Cu-Al_2O_3-g-C_3N_4 (Fig. 4A) and 285.7 eV of Cu-Al_2O_3-C-dots (Fig. 4B) are ascribed to the C atoms of the aromatic ring bonded to the hydroxyl groups (C—O—H/C—O—metal). Based on the analysis of the XPS spectra, we could confirm the existence of the C—O— bond between the g-C_3N_4/C-dots and the surface Cu, which is also in agreement with the FT-IR spectra of Cu-Al_2O_3-g-C_3N_4 and Cu-Al_2O_3-C-dots. In addition, for the O 1s spectra (Fig. S6), the two peaks at 530.9–531.7 eV and 532.8–533.0 eV correspond to lattice oxygen and surface adsorbed oxygen, respectively.

To obtain deep insight into the electronic structural information of paramagnetic Cu(II), solid electron paramagnetic resonance (EPR) spectra of catalysts were comparatively analysed (Fig. 5). EPR signals with the hyperfine coupling of Cu-Al_2O_3, Cu-Al_2O_3-g-C_3N_4, and Cu-Al_2O_3-C-dots were clearly observed, suggesting the presence of Cu(II) with I (nuclear spin) = 3/2 (room temperature). For all samples, the trend of $g\| > g\perp > 2.0023$ (g_e) indicated that the lone paired electron was localized in the dx^2-y^2 orbital of Cu(II) [33], also confirming the formation of the electron-rich copper centre. Previous studies have systematically reported the relationships between the EPR signal shape and the coordination structure of Cu(II) [30]. The EPR signal shape (Cu-Al_2O_3, Cu-Al_2O_3-g-C_3N_4, and Cu-Al_2O_3-C-dots) could correspond to the

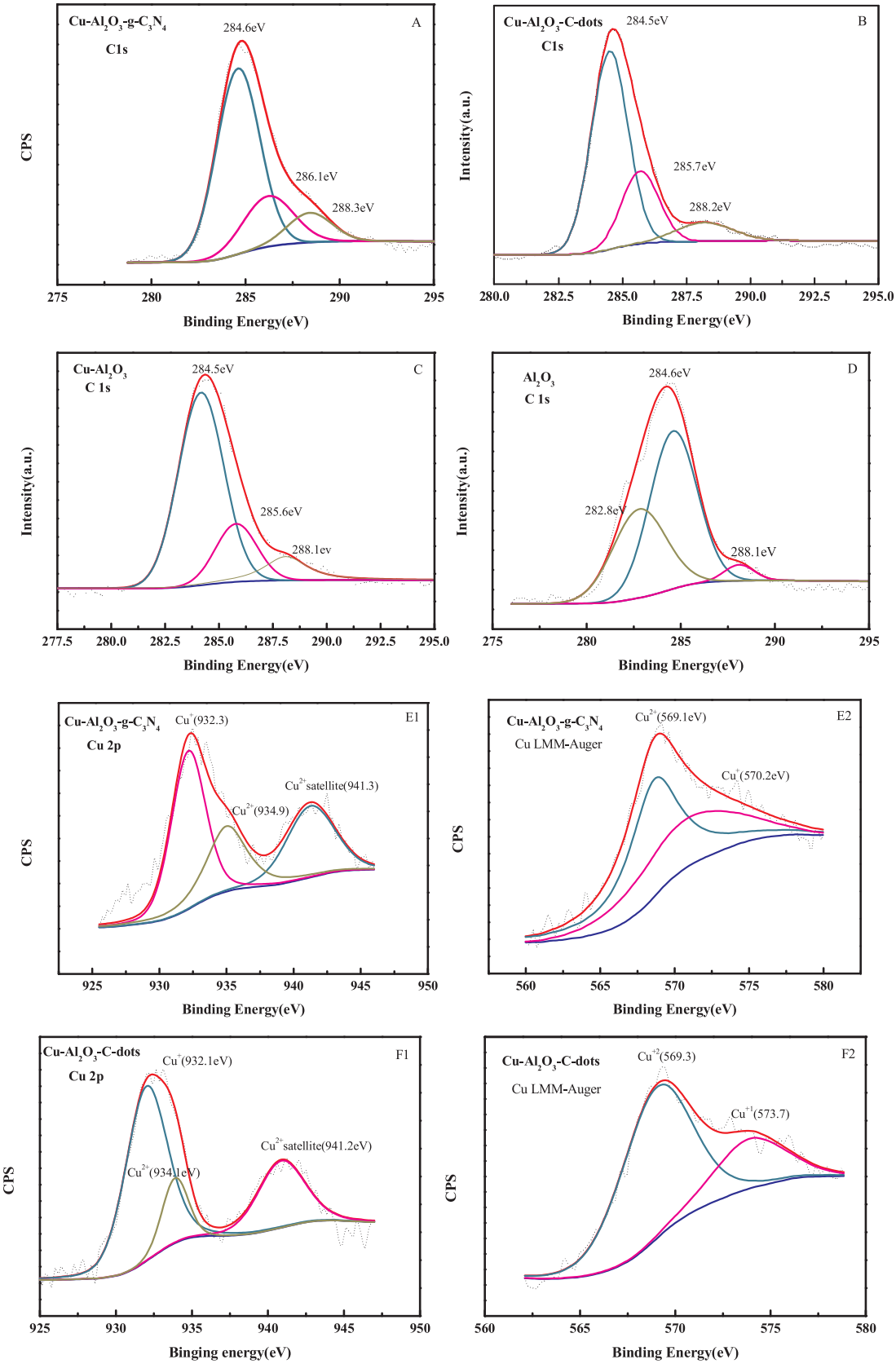

Fig. 4. XPS spectra in C 1s for (A) Cu-Al_2O_3-g-C_3N_4 (B) Cu-Al_2O_3-C-dots (D) Cu-Al_2O_3 (D) Al_2O_3, (E1) Cu 2p for Cu-Al_2O_3-g-C_3N_4, (F1) Cu-Al_2O_3-C-dots, LMM X-ray induced Auger kinetic energy for (E2) Cu-Al_2O_3-g-C_3N_4, (F2) Cu-Al_2O_3-C-dots.

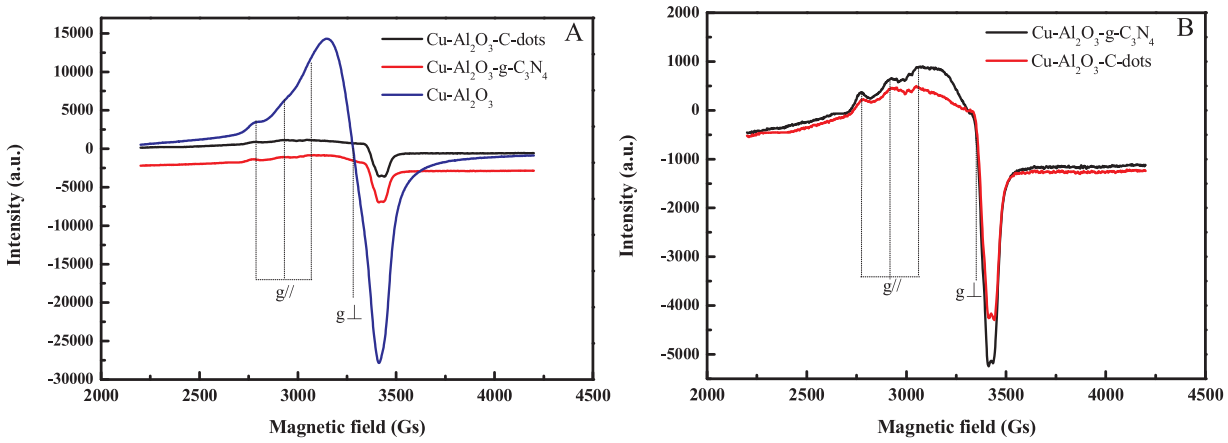

Fig. 5. (A) Solid EPR spectra of Cu-Al_2O_3, Cu-Al_2O_3-g-C_3N_4, and Cu-Al_2O_3-C-dots (B) Enlargement of solid EPR spectra of Cu-Al_2O_3-g-C_3N_4, and Cu-Al_2O_3-C-dots.

six-coordinated Cu(II) with an octahedral geometry. Notably, after the introduction of g-C_3N_4 and C-dots, the intensity of the EPR signals was significantly decreased. This phenomenon could be explained as follows: both g-C_3N_4 and C-dots promoted the migration of free electrons to the copper centre via Cu(II)–π interactions (Cu—O—C bond). On the other hand, as the indicator of the amount of Cu(II) and free electrons density around copper, the decrease in the intensity of the EPR signal was ascribed to the increase in the electron density around copper, providing a more clear indication of the reduced state.

3.2. Catalytic performance

Catalytic degradation of Rh B was used for the comparative evaluation of the catalytic activities of Al_2O_3, Fe-Al_2O_3 and Cu-Al_2O_3. To

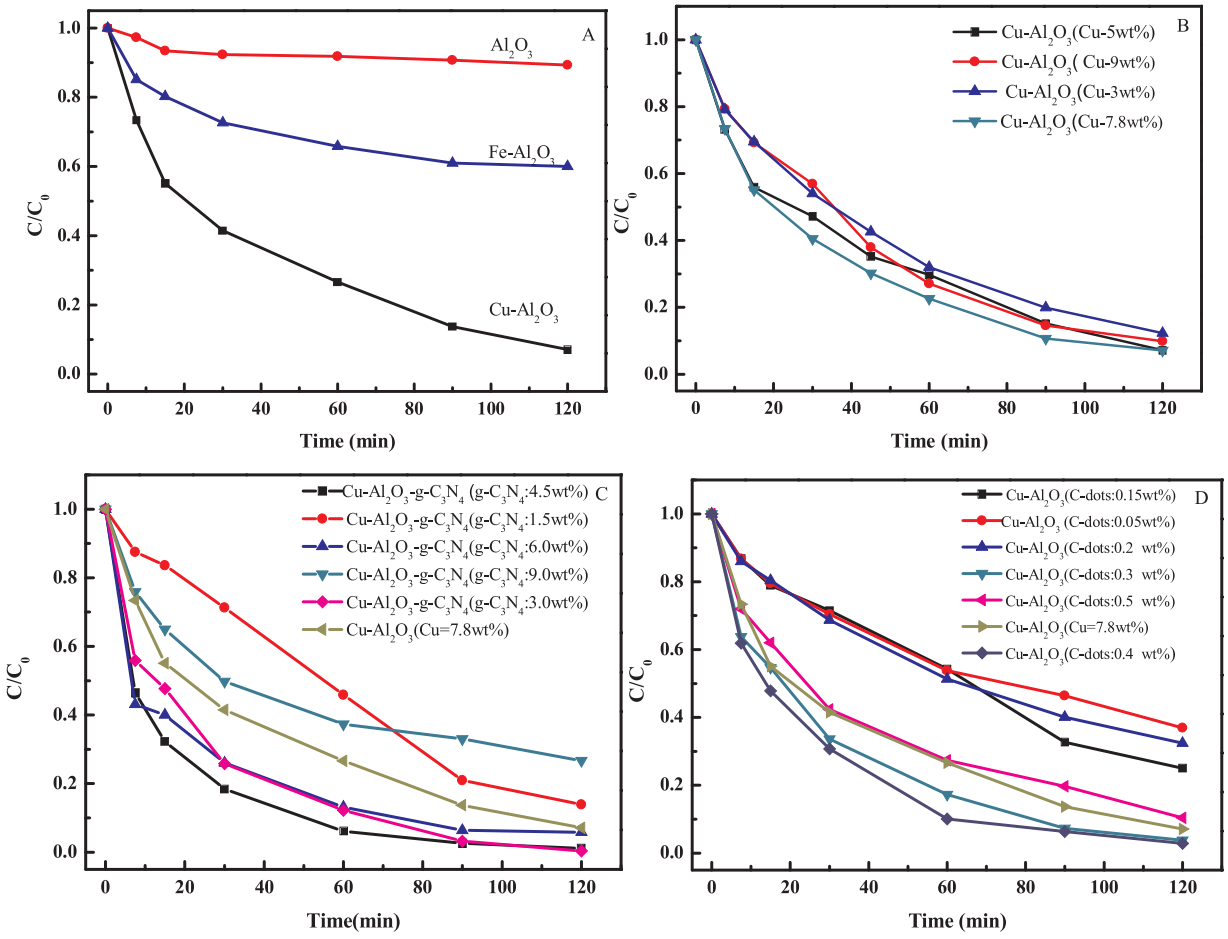

Fig. 6. Optimizing the catalyst composites based on the evaluation of Fenton degradation rate of Rh B (A) Fenton degradation of Rh B in Al_2O_3, Fe-Al_2O_3, Cu-Al_2O_3 (Cu: 7.8 wt%) suspensions.(B) Effect of the amount of the introduced Cu during the preparation of Cu-Al_2O_3 on Rh B degradation. (C) Effect of the amount of the g-C_3N_4 during the preparation of Cu-Al_2O_3-g-C_3N_4 on Rh B degradation (Cu: 7.8 wt%). (D) Effect of the amount of the C-dots during the preparation of Cu-Al_2O_3-C-dots (Cu: 7.8 wt%) on Rh B degradation.(Initial pH 7, initial Rh B concentration 10 mg/L, initial H_2O_2 concentration 12.5 mM, catalyst 0.5 g/L.

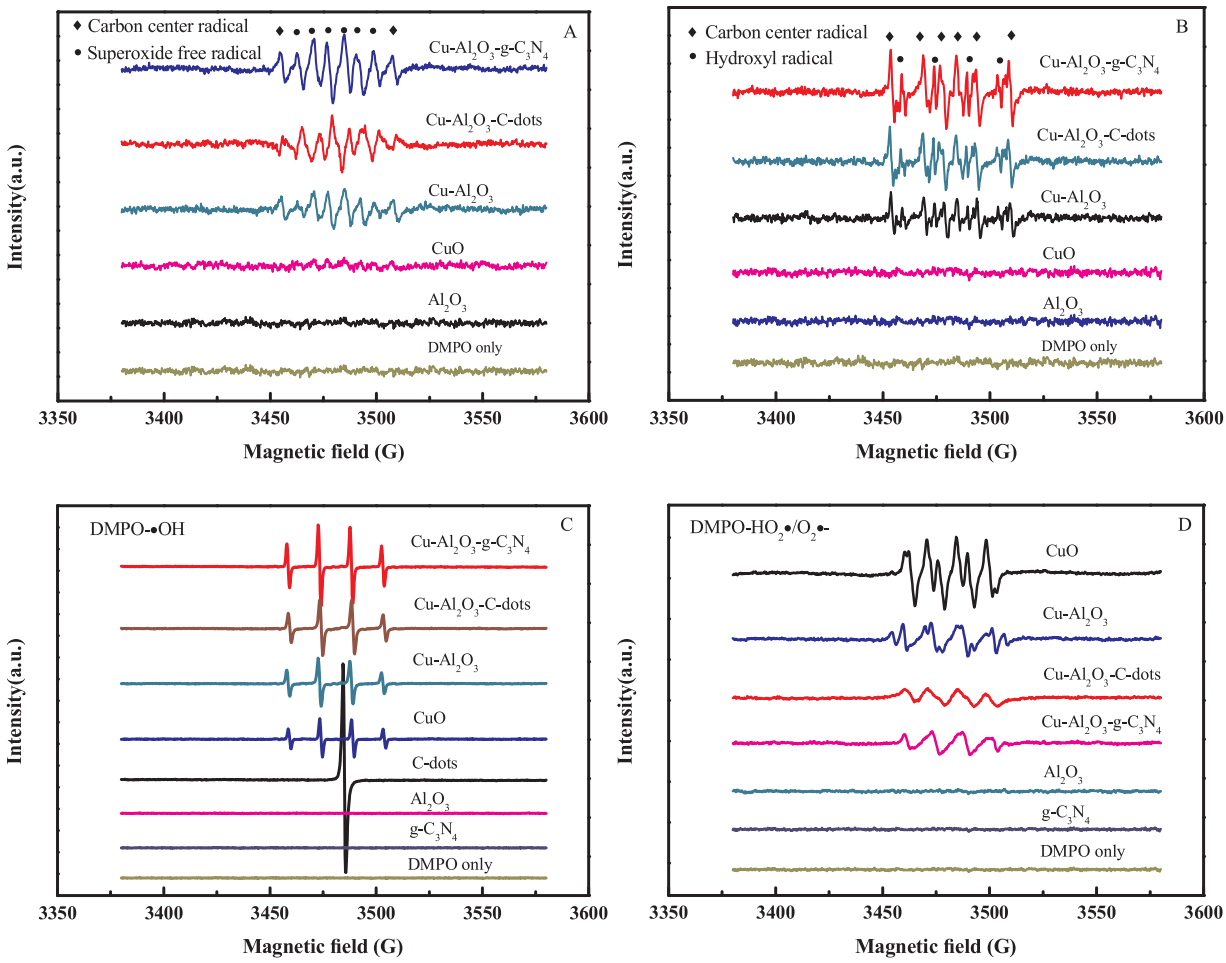

Fig. 7. DMPO spin-trapping EPR spectra for (A) $HO_2\cdot/O_2\cdot^-$ in various methanol dispersions and (B) ·OH in various methanol dispersions without H_2O_2. (C) ·OH in various aqueous suspensions and (D) $HO_2\cdot/O_2\cdot^-$ in various methanol dispersions in the presence of H_2O_2.

exclude the influence of the adsorption capacity of the catalyst on the Rh B removal, 24.2%, 24.7% and 25.5% of Rh B (10 ppm) were pre-adsorbed on Al_2O_3, Fe-Al_2O_3 and Cu-Al_2O_3 prior to the addition of H_2O_2. In the presence of H_2O_2 (Fig. 6A), approximately 8%, 40% and 92% of BPA are degraded within 45 min in the Al_2O_3, Fe-Al_2O_3 and Cu-Al_2O_3 suspensions, respectively. Thus, Cu-Al_2O_3 exhibited a much higher catalytic activity in neutral conditions than Al_2O_3 and Fe-Al_2O_3. Furthermore, the catalytic activities of Cu-Al_2O_3 with various Cu contents (3, 5, 7.8, and 9 wt%) are tested, indicating that the catalysts activities follow the order of 7.8 wt% > 5 wt% > 9 wt% > 3 wt% (Fig. 6B). During the hydrothermal reaction process, some copper was incorporated into the framework of the Cu-Al_2O_3, while other copper ions were present as the extra framework copper species. Owing to the existence of an upper limit for the amount of copper that could be incorporated inside the framework [34], further increase of the copper content would lead to additional extra framework copper species. Notably, the framework copper species were more stable than the extra framework species [35], and excessive amounts of extra framework copper species may impede the contact between H_2O_2 and framework copper species during the Fenton-like reaction [36]. Thus, Cu-Al_2O_3 (7.8 wt%) exhibited the highest catalytic activity and was selected as the optical catalyst for further studies.

Compared with Cu-Al_2O_3, Cu-Al_2O_3-g-C_3N_4 and Cu-Al_2O_3-C-dots show higher catalytic activity for Fenton-like degradation of Rh B (Fig. 6C and D). The catalytic activities of Cu-Al_2O_3-g-C_3N_4 with various g-C_3N_4 content followed the order of 4.5 wt% > 3.0 wt% > 6 wt % > 0 wt% > 1.5 wt% > 9 wt% (Fig. 6C). Although g-C_3N_4 loaded on catalysts could increase the removal rate of Rh B, excess of g-C_3N_4 loaded on catalysts might aggregate to clusters and partially wrap the active site on the catalysts. Thus, Cu-Al_2O_3-g-C_3N_4 (g-C_3N_4: 4.5 wt%) showed the highest catalytic activity. Furthermore, the catalytic activities of Cu-Al_2O_3-C-dots with various C-dots content followed the order of 0.4 wt% > 0.3 wt% > 0 wt% > 0.5 wt% > 0.15 wt% > 0.2 wt % > 0.05 wt% (Fig. 6D), which indicates that loading of C-dots could increase the removal rate of Rh B. However, higher amount of C-dots might aggregate to clusters and then inhibit the electrons transfer process [37]. Consequently, Cu-Al_2O_3-g-C_3N_4 (g-C_3N_4: 4.5 wt%) and Cu-Al_2O_3-C-dots (C-dots: 0.4 wt%) were selected for the subsequent experiments.

The effects of catalysts' (Cu-Al_2O_3-g-C_3N_4, Cu-Al_2O_3-C-dots) concentration on BPA degradation are investigated in the present work (Fig. S7). In the absence of the catalyst, BPA could not be degraded. By contrast, approximately 84%, 87% and 92% of BPA are degraded with the catalysts' concentrations of 0.3, 0.5 and 0.8 g/L within 20 min, respectively (Fig. S7A). Meanwhile, approximately 77%, 82%, and 92% of BPA was degraded within 20 min at the Cu-Al_2O_3-C-dots concentrations of 0.3, 0.5 and 0.8 g/L, respectively (Fig. S7B). These results indicated that although the degradation of BPA was improved with increased catalyst concentration, BPA removal could not be significantly enhanced for the catalyst concentration of more than 1.0 g/L. In addition, the influence of H_2O_2 concentration on the catalytic degradation process is also tested with the catalysts concentration of 0.5 g/L (Fig. S7C). It was found that only 5% of BPA was degraded in the absence of H_2O_2 within 30 min, while BPA degradation was significantly improved in the presence of H_2O_2. More than 97.3% BPA was removed as 12.5 mM H_2O_2 was added into Cu-Al_2O_3-g-C_3N_4 suspension

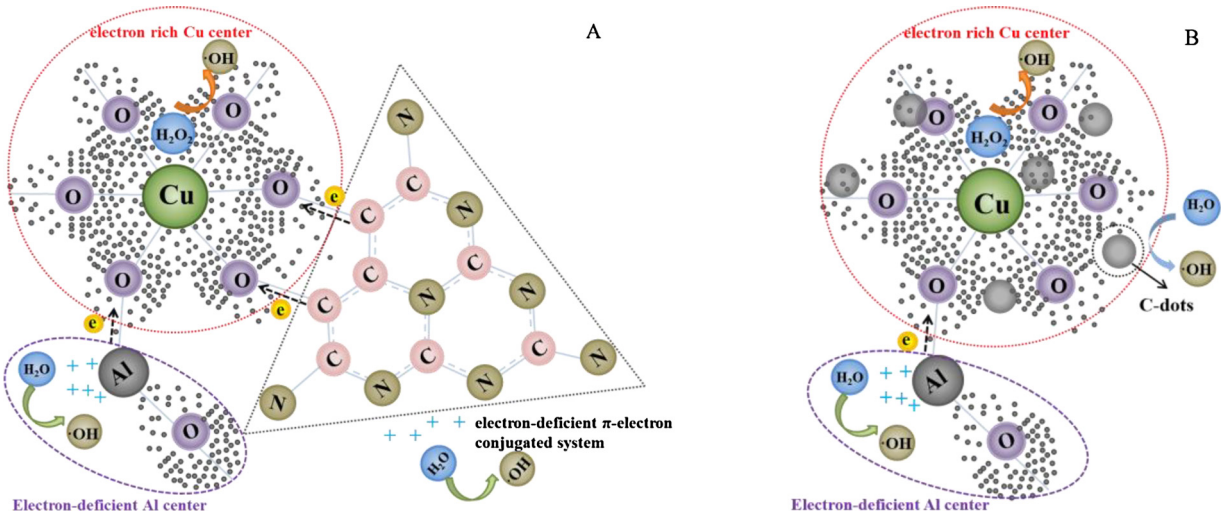

Fig. 8. The Fenton-like reaction mechanism on the surface of (A) Cu-Al_2O_3-g-C_3N_4 and (B) Cu-Al_2O_3-C-dots.

within 30 min. However, the degradation rate of BPA would not increase obviously for H_2O_2 concentration greater than 20 mM. A similar phenomenon was observed when we tested the effect of the H_2O_2 concentration on the degradation of BPA over Cu-Al_2O_3-C-dots (Fig. S7D).

The adaptability of two catalysts to different kinds of pollutants under neutral conditions was systematically tested, and it was found that more than 80% of organic pollutants [Rhodamine B (Rh B), methylene blue (MB), 2,4-dichlorophenoxyacetic acid (2,4-D) and phenytoin sodium (PHT)] can be removed within 90 min (Fig. S10). Furthermore, the leaching of copper and aluminium during the reaction process is lower than the limitations specified by the EU and US (< 2 ppm) (Fig. S8A). In addition, to investigate the effect of dissolved copper on the catalytic degradation process, a homogeneous experiment using 0.35 mg/L Cu(II) with 12.5 mM H_2O_2 was conducted. It was found that only 13.5% BPA is removed within 120 min (Fig. S8B), suggesting that BPA removal over the catalysts (Cu-Al_2O_3-g-C_3N_4 and Cu-Al_2O_3-C-dots) is mainly due to heterogeneous catalytic reactions.

To evaluate their potentials in practical application, the stabilities of Cu-Al_2O_3-g-C_3N_4 and Cu-Al_2O_3-C -dots were tested (Fig. S9). The catalytic activities of Cu-Al_2O_3-g-C_3N_4 and Cu-Al_2O_3-C-dots did not decrease obviously, remaining at approximately 91% and 89% within 60 min after 7 successive cycles, respectively. Thus, Cu-Al_2O_3-g-C_3N_4 and Cu-Al_2O_3-C-dots may be used as promising Fenton-like catalysts for the degradation of organic pollutants in the future.

3.3. Catalytic mechanism

To further elucidate the catalytic mechanism, DMPO-trapped EPR signals were detected in different air-saturated methanol/aqueous dispersions of the corresponding samples without the addition of H_2O_2 (Fig. 7). Six characteristic peaks of DMPO–$O_2\cdot^-$ were observed in the methanol dispersions of catalysts with their intensities following the order of $Cu-Al_2O_3-g-C_3N_4$ > Cu-Al_2O_3-C-ots > Cu-Al_2O_3. However, no signals were observed in the system of Al_2O_3 methanol dispersion, unmodified CuO methanol dispersion and the blank experiment (Fig. 7A). In addition, the other peaks were assigned to the carbon centre radicals generated from the reaction between DMPO and $O_2\cdot^-$ [38]. Since these peaks overlapped with the $HO_2\cdot/O_2\cdot^-$ characteristic peak, they could not be completely identified from the EPR spectra. The EPR spectra suggested that Cu was incorporated in the lattice of Al_2O_3 and substitutes a fraction of Al in the Cu-Al_2O_3 system. Accordingly, different electro-negativities of the metals (Cu, Al) led to the non-uniform electron density distribution of the lattice O^{2-}. Transferring from the lattice O^{2-} (Cu—O—Al), a higher electron density was formed around Cu, while a lower electron density appeared in the region around Al. El ectrons around the electron-rich Cu centre of Cu-Al_2O_3 could reduce O_2 (in methanol dispersions) to $O_2\cdot^-$ [39]. Notably, the four characteristic peaks of DMPO–·OH follow the order of Cu-Al_2O_3-g-C_3N_4 > Cu-Al_2O_3-C-dots > Cu-Al_2O_3 (Fig. 7B). The other six peaks were ascribed to the carbon-centred radical adduct, which resulted from the attack of carbon-containing compounds by ·OH [40]. Similar to DMPO–$HO_2\cdot/O_2\cdot^-$, no signals of ·OH were observed in the Al_2O_3 methanol dispersion, unmodified CuO methanol dispersion and the blank experiment. It is revealed that in the Cu-Al_2O_3 system, the electron-deficient Al centre could accept the electron from H_2O and then oxide H_2O to produce ·OH radicals.

Moreover, the $HO_2\cdot/O_2\cdot^-$ and ·OH intensity of Cu-Al_2O_3-g-C_3N_4 and Cu-Al_2O_3-C-dots was higher than that of Cu-Al_2O_3, indicating that the Cu centre of Cu-Al_2O_3-g-C_3N_4 and Cu-Al_2O_3-C-dots possessed more unpaired electrons than the Cu centre of Cu-Al_2O_3, resulting in reduction of more O_2 to $O_2\cdot^-$ in the Cu-Al_2O_3-g-C_3N_4 system. Electron transport via π→Cu (σ donation) led to greater electron accumulation around the Cu centre via the bond linkage (Cu—O—C) between Cu-Al_2O_3 and the hydroxyl of the aromatic ring (g-C_3N_4 or C-dots). Meanwhile, the double electron-deficient centres (the Cu-Al_2O_3 system and the π-conjugated graphitic planes) of Cu-Al_2O_3-g-C_3N_4 and Cu-Al_2O_3-C-dots could accept the electrons from H_2O and then oxidize H_2O to generate more ·OH radicals compared to Cu-Al_2O_3.

In the presence of H_2O_2 (Fig. 7C and D), the main products are ·OH radicals with the signal intensity in the order of Cu-Al_2O_3-g-C_3N_4 > Cu-Al_2O_3-C-dots > Cu-Al_2O_3 > CuO, while the signal intensity of $O_2\cdot^-$ radicals follow the order of CuO > Cu-Al_2O_3 > Cu-Al_2O_3-C-dots > Cu-Al_2O_3-g-C_3N_4. These results indicated that H_2O_2 was mainly reduced to ·OH by the electrons around the Cu centres of Cu-Al_2O_3, Cu-Al_2O_3-C-dots and Cu-Al_2O_3-g-C_3N_4. Notably, in unmodified CuO aqueous suspensions, because the decomposition of H_2O_2 followed the classic Fenton reaction mechanism, H_2O_2 was not only reduced to ·OH but also oxidized to large amounts of $O_2\cdot^-$. Such different decomposition mechanism of H_2O_2 led to higher selective H_2O_2 conversion to hydroxyl radicals over Cu-Al_2O_3-C-dots and Cu-Al_2O_3-g-C_3N_4. In addition, the ·OH intensity of Cu-Al_2O_3-g-C_3N_4 and Cu-Al_2O_3-C-dots was obviously higher than that of Cu-Al_2O_3, further confirming the improvement of catalytic activity and H_2O_2 utilization.

Fig. 8 clearly illustrates the generation mechanisms of ·OH over Cu-Al_2O_3-g-C_3N_4 and Cu-Al_2O_3-C-dots. Cu ions could coordinate with hydroxyl on the tri-s-triazine ring of g–C_3N_4 or on the graphene conjugated π-domains of C-dots, inducing the formation of an electron-rich Cu centre and an electron-deficient π-electron conjugated system via the C-O-Cu bond, which strengthened the dual-reaction centres (Cu and

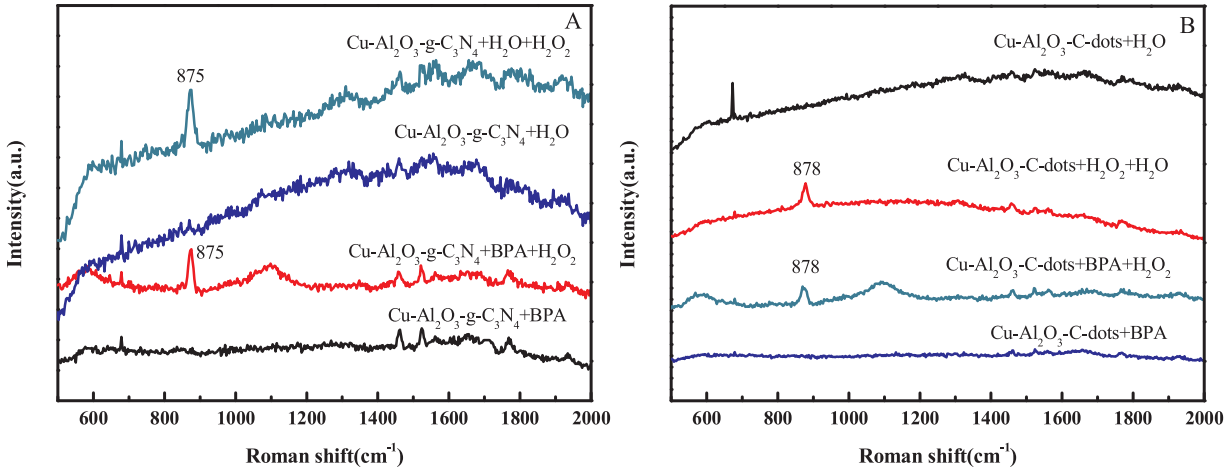

Fig. 9. In situ Raman spectra for various catalyst aqueous dispersions (A) Cu-Al_2O_3-g-C_3N_4 (B) Cu-Al_2O_3-C-dots.

Al). Thus, there were two electron transfer routes to generate ·OH in the presence of H_2O_2: the first route was from the electron-rich Cu centres to H_2O_2, and the second route was from H_2O to the electron-deficient site. Consequently, more ·OH was generated and high utilization of H_2O_2 was achieved in the Cu-Al_2O_3-g-C_3N_4 and in Cu-Al_2O_3-C-dots suspension.

The interaction processes between the corresponding samples and H_2O_2 were also confirmed by Raman spectroscopy (Fig. 9). Regardless of whether the BPA was added, only the system Raman bands were observed in the absence of H_2O_2. However, as H_2O_2 was added in the suspensions of Cu-Al_2O_3-g-C_3N_4 (Fig. 9A) and Cu-Al_2O_3-C-dots (Fig. 9B), a new band corresponding to the O—O stretching for the peroxo complexes of H_2O_2 with metal ions appeared at 876–881 cm^{-1} [41,42]. Molecular H_2O_2 could act as a dipole (an electrophilic or nucleophilic agent) owing to its structure [16]. As Cu was incorporated in the framework of Al_2O_3, the higher electro-negativity of Cu led to the nonuniform distribution of the electron density of the lattice O^{2-}. Consequently, two species of adsorption sites for H_2O_2/BPA were formed: the first was the electron-rich region around the lattice Cu, and the second was the electron-deficient region around the lattice Al. Especially, Cu ions coordinate with hydroxyl on the tri-s-triazine ring of g–C_3N_4 and the hydroxyl on the graphene conjugated π-domains of C-dots, which induce the formation of an electron-rich Cu centre and an electron-deficient π-electron conjugated system, resulting in the strengthening of the dual-reaction centres.

In the absence of BPA, H_2O_2 may be absorbed on the electron-deficient region of the catalyst, acts as the electron donor and is finally decomposed into HO_2·/O_2·$^-$ and O_2. As BPA was added in the dispersion, the absorption bands of Cu-Al_2O_3-g-C_3N_4 and Cu-Al_2O_3-C-dots mentioned above decreased. This was because BPA could partly occupy the electron-deficient region and acted as the electron donor, which prevented the nucleophilic H_2O_2 from combining with this site of the catalysts. Therefore, H_2O_2 was predominantly adsorbed on the electron-rich region and then was reduced to ·OH, resulting in the high H_2O_2 utilization efficiency.

Generally, the utilization of H_2O_2 (η) in Fenton reaction could be evaluated by the ratio of the stoichiometric H_2O_2 consumption ($[H_2O_2]_S$) for the pollutant mineralization with the actual H_2O_2 consumption ($[H_2O_2]_A$) [43]. As shown in Table 1, the H_2O_2 utilization efficiencies by various catalysts follow the order of Cu-Al_2O_3-g-C_3N_4 (64%) > Cu-Al_2O_3-C-dots (59%) > Cu-Al_2O_3 (47%) > CuO (28%), which are in accordance with the order of TOC removal [Cu-Al_2O_3-g-C_3N_4 (72.3%) > Cu-Al_2O_3-C-dots (68.1%) > Cu-Al_2O_3(59.7%) > CuO (23.8%)] (Fig. S11).

To directly illustrate the relationship between the generation of ·OH and consumption of H_2O_2, ·OH produced in the aqueous dispersion with H_2O_2 was quantitatively measured using the terephthalic acid (TPA) probe method (detailed information provided in the ESI). The production of ·OH within 120 s was approximately 1.5, 1.3 and 1.1 times higher than the H_2O_2 consumption in the Cu-Al_2O_3-g-C_3N_4, Cu-Al_2O_3-C-dots and Cu-Al_2O_3 systems, respectively. Within 600 s, the production of ·OH still remains higher than the H_2O_2 consumption (Fig. 10A). However, with the increase in the reaction time, a fraction of ·OH could react with the intermediates of the degraded TPA, H_2O_2 and ·OH itself involving the free radical chain reactions, resulting in a lower measurement value.

Table 1
Actual H_2O_2 consumption ($[H_2O_2]_A$) and stoichiometric H_2O_2 consumption ($[H_2O_2]_S$) for mineralizing BPA (20 mg L^{-1}) during the Fenton-like reaction.

catalyst	Time (min)	TOC removal (mg/L)	$[\Delta H_2O_2]_A$ (mM)	$[\Delta H_2O_2]_S$ (mM)	η[H_2O_2] (%)
CuO	120	23.8%	2.69	0.75	28%
Cu-Al_2O_3	120	59.7%	4.31	2.03	47%
Cu-Al_2O_3-g-C_3N_4	120	72.3%	3.57	2.28	64%
Cu-Al_2O_3-C-dots	120	68.1%	3.62	2.14	59%

In addition, the amount of electron-rich Cu centres was related to the amount of the Cu element dispersed on the catalyst surface. Since phenol could be adsorbed on the surface of Cu-Al_2O_3 owing to the complexation between phenol and Cu, the maximum theoretical monolayer adsorption capacity of phenol on Cu-Al_2O_3 can be considered as the amount of the electron-rich Cu centres of the catalysts. By using the Langmuir equation to fit the adsorption isotherms of phenol on Cu-Al_2O_3 (Fig. 10B), the maxim theoretical monolayer adsorption capacity for phenol ($q_e = 0.61 \times 10^{-5}$ mol/g) is calculated, which can be considered as the amount of Cu distributed on the surface of Cu-Al_2O_3, Cu-Al_2O_3-C-dots and Cu-Al_2O_3-g-C_3N_4 (detailed information of Langmuir adsorption equation was provided in the ESI). Consequently, the turnover frequency (TOF) values of Cu-Al_2O_3, Cu-Al_2O_3-C-dots and Cu-Al_2O_3-g-C_3N_4 can be calculated by Eq. 3 and are found to be 0.380 s^{-1}, 0.461 s^{-1} and 0.516 s^{-1}, respectively. Owing to the free radical chain reaction, the calculated values of TOF were lower than the actual values. Nonetheless, the TOF values of the Cu–Al_2O_3–C–dots and Cu–Al_2O_3–g–C_3N_4 dispersions under neutral conditions were still 30 times and 34 times higher than those of the classic homogeneous Fenton reaction under strongly acidic conditions (1.53×10^{-2} s^{-1}) [44]. Thus, Cu-Al_2O_3-g-C_3N_4 and Cu-Al_2O_3-C-dots could significantly enhance the selective H_2O_2 conversion to hydroxyl radicals compared to the classic Fenton catalysts.

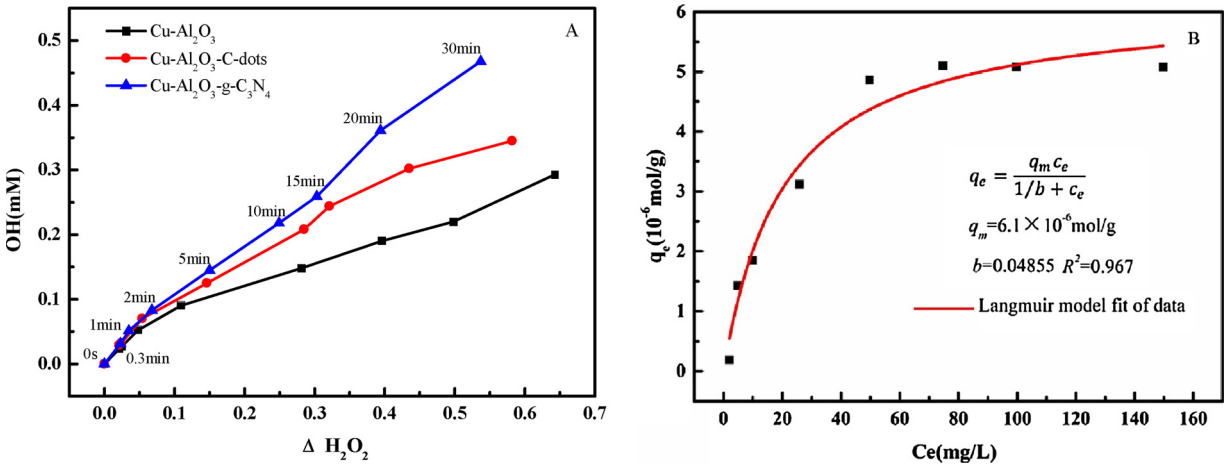

Fig. 10. Calculation of TOFs of H_2O_2 by using TPA method (A) Measurement of the generation of ·OH using the TPA method (initial TPA 665 mg L^{-1}). (B) Adsorption isotherms of phenol on Cu-Al_2O_3 (initial phenol: 2–150 mg L^{-1}, adsorbent addition: 0.5 g L^{-1}, pH = 7).

$$TOF = V(\cdot OH)\cdot N_A/[C(catal.)\cdot N(surf.)] \quad (3)$$

where *C(catal.)* is the concentration of the catalyst (0.5 g/L), *V*(·OH) is the generation rate of ·OH, *N(surf.)* is the number of active sites on the surface of the catalyst and N_A is the Avogadro constant (6.02×10^{23}).

4. Conclusions

Two novel Fenton-like catalysts Cu-Al_2O_3-g-C_3N_4 and Cu-Al_2O_3-C-dots with the dual-reaction centres were prepared with high activity and H_2O_2 utilization efficiency for the degradation and mineralization of organic pollutants under neutral pH conditions. In the Cu-Al_2O_3-g-C_3N_4 and Cu-Al_2O_3-C-dots system, the electron-rich centre of Cu and electron-deficient site of Al were formed. Moreover, Cu ions could coordinate with hydroxyl on the tri-s-triazine ring of g–C_3N_4 or on the graphene conjugated π-domains of C-dots, inducing the formation of an electron-rich Cu centre and an electron-deficient π-electron conjugated system, which strengthened the dual-reaction centres. There were two electron transfer routes for the generation of ·OH in the presence of H_2O_2: the first was from the electron-rich Cu centres to H_2O_2, and the second was from H_2O to the electron-deficient site. Thus, more ·OH were generated and high H_2O_2 utilization was achieved in the Cu-Al_2O_3-g-C_3N_4 and Cu-Al_2O_3-C-dots suspension. The turnover frequency (TOF) values of Cu–Al_2O_3–C–dots (0.461 s^{-1}) and Cu–Al_2O_3–g–C_3N_4 (0.516 s^{-1}) dispersions were much higher than those of the classic homogeneous Fenton reaction (0.0153 s^{-1}) under strongly acidic conditions. Thus, Cu-Al_2O_3-g-C_3N_4 and Cu-Al_2O_3-C-dots could significantly enhance the selective H_2O_2 conversion to hydroxyl radicals compared with the classic Fenton catalysts. In summary, the present work not only prepared novel Fenton-like catalysts with high activity and stability for catalytic degradation of organic pollutants under mild conditions but also provided a simple method to construct electron-rich areas for the selective conversion of H_2O_2 to ·OH.

Acknowledgements

This research was supported by Water Resource Research Project of Jiangsu Province (2016039), the Fundamental Research Funds for the Central Universities (0211-14380065) and the State Key Program of National Natural Science of China (No. 51438008).

Appendix A. Supplementary data

Supplementary material related to this article can be found, in the online version, at doi:https://doi.org/10.1016/j.apcatb.2018.04.029.

References

[1] M. Hartmann, S. Kullmann, H. Keller, J. Mater. Chem. 20 (2010) 9002–9017.
[2] H. Lim, J. Lee, S. Jin, J. Kim, J. Yoon, T. Hyeon, Chem. Commun. (2006) 463–465.
[3] Y. Feng, C.Z. Liao, K.M. Shih, Chemosphere 154 (2016) 573–582.
[4] R.C.C. Costa, M.F.F. Lelis, L.C.A. Oliveira, J.D. Fabris, J.D. Ardisson, R. Rios, C.N. Silva, R.M. Lago, J. Hazard. Mater. 129 (2006) 171–178.
[5] X.F. Li, X. Liu, L.L. Xu, Y.Z. Wen, J.Q. Ma, Z.C. Wu, Appl. Catal. B: Environ. 165 (2015) 79–86.
[6] L. Lyu, L. Zhang, Q. Wang, Y. Nie, C. Hu, Environ. Sci. Technol. 49 (2015) 8639–8647.
[7] W.J. Song, M.M. Cheng, J.H. Ma, W.H. Ma, C.C. Chen, J.C. Zhao, Environ. Sci. Technol. 40 (2006) 4782–4787.
[8] Z. Jia, J. Kang, W.C. Zhang, W.M. Wang, C. Yang, H. Sun, D. Habibi, L.C. Zhang, Appl. Catal. B: Environ. 204 (2017) 537–547.
[9] S. Huang, Y. Xu, T. Zhou, M. Xie, Y. Ma, Q. Liu, L. Jing, H. Xu, H. Li, Appl. Catal. B: Environ. 225 (2018) 40–50.
[10] Y. Wang, H. Zhao, M. Li, J. Fan, G. Zhao, Appl. Catal. B: Environ. 147 (2014) 534–545.
[11] Y. Zhong, X. Liang, Y. Zhong, J. Zhu, S. Zhu, P. Yuan, H. He, J. Zhang, Water Res. 46 (2012) 4633–4644.
[12] J.F. Perez-Benito, J. Inorg. Biochem. 98 (2004) 430–438.
[13] L. Lai, L. Zhang, C. Hu, M. Yang, J. Mater. Chem. A 4 (2016) 8610–8619.
[14] I. Sires, J.A. Garrido, R.M. Rodriguez, P.I. Cabot, F. Centellas, C. Arias, E. Brillas, J. Electrochem. Soc. 153 (2006) D1–D9.
[15] R. Salazar, E. Brillas, I. Sirés, Appl. Catal. B: Environ. 115 (2012) 107–116.
[16] L. Lai, L. Zhang, C. Hu, Environ. Sci.: Nano 3 (2016).
[17] L. Lyu, L. Zhang, G. He, H. He, C. Hu, J. Mater. Chem. A 5 (2017) 7153–7164.
[18] A. Lagutschenkov, R.K. Sinha, P. Maitre, O. Dopfer, J. Phys. Chem. A 114 (2010) 11053–11059.
[19] Y. Wang, X. Wang, M. Antonietti, Cheminform 51 (2012) 68.
[20] J. Shen, Y. Zhu, C. Chen, X. Yang, C. Li, Chem. Commun. 47 (2011) 2580–2582.
[21] A. Nourbakhsh, M. Cantoro, T. Vosch, G. Pourtois, F. Clemente, M.H. van der Veen, J. Hofkens, M.M. Heyns, S. De Gendt, B.F. Sels, Nanotechnology 21 (2010).
[22] V.F. Lapko, I.P. Gerasimyuk, V.S. Kuts', Y.A. Tarasenko, Russ. J. Phys. Chem. A 84 (2010) 934–940.
[23] W.J. Ong, L.L. Tan, Y.H. Ng, S.T. Yong, S.P. Chai, Chem. Rev. 116 (2016) 7159–7329.
[24] H. Ming, Z. Ma, Y. Liu, K. Pan, H. Yu, F. Wang, Z. Kang, Dalton Trans. 41 (2012) 9526–9531.
[25] H. Bader, V. Sturzenegger, J. Hoigne, Water Res. 22 (1988) 1109–1115.
[26] H. Liu, G. Lu, Y. Guo, Y. Wang, Y. Guo, Open Chem. 7 (2009).
[27] S. Guo, D. Li, L. Zhang, J. Li, E. Wang, Biomaterials 30 (2009) 1881–1889.
[28] Y. Guo, X. Liu, X. Wang, A. Iqbal, C. Yang, W. Liu, W. Qin, RSC Adv. 5 (2015) 95495–95503.
[29] A. Lagutschenkov, R.K. Sinha, P. Maitre, O. Dopfer, J. Phys. Chem. A 114 (2010) 11053–11059.
[30] X. Sun, Y. Li, Angew. Chem. 116 (2010) 607–611.
[31] A.C. Lua, T. Yang, J. Colloid Interface Sci. 274 (2004) 594.
[32] Y. Zhang, Z. Liu, D. Zang, L. Feng, Vacuum 99 (2014) 160–165.
[33] R.-R. Cheng, Z.-L. Wu, Y.-L. Hou, J. Dong, J.-Z. Cui, B. Zhao, Inorg. Chem. Commun. 51 (2015) 95–98.
[34] L. Fu, H. Yang, J. Phys. Chem. C 118 (2014) 14299–14315.
[35] L. Zhang, D. Xu, C. Hu, Y. Shi, Appl. Catal. B: Environ. 207 (2017) 9–16.
[36] L. Lyu, L. Zhang, C. Hu, Chem. Eng. J. 274 (2015) 298–306.
[37] X. Tian, H. Jin, Y. Nie, Z. Zhou, C. Yang, Y. Li, Y. Wang, Chem. Eng. J. 328 (2017) 397–405.
[38] L. Wang, F. Wang, P. Li, L. Zhang, Sep. Purif. Technol. 120 (2013) 148–155.
[39] L. Lyu, D. Yan, G. Yu, W. Cao, C. Hu, Environ. Sci. Technol. (2018).
[40] L. Khachatryan, B. Dellinger, Environ. Sci. Technol. 45 (2011) 9232–9239.
[41] S. Bordiga, A. Damin, F. Bonino, G. Ricchiardi, C. Lamberti, A. Zecchina, Angew. Chem. Int. Ed. 41 (2002) 4734–4737.
[42] M.L. Kuznetsov, Y.N. Kozlov, D. Mandelli, A.J.L. Pombeiro, G.B. Shul'pin, Inorg. Chem. 50 (2011) 3996–4005.
[43] L. Lai, G. Yu, L. Zhang, C. Hu, Y. Sun, Environ. Sci. Technol. 52 (2018) 747–756.
[44] X. Huang, X. Hou, J. Zhao, L. Zhang, Appl. Catal. B: Environ. 181 (2016) 127–137.